Radio Map-Based Cognitive Satellite-UAV Networks Towards 6G On-Demand Coverage

Wei Feng, *Senior Member, IEEE,* Yueshan Lin, Yanmin Wang, Jue Wang, *Member, IEEE,*
Yunfei Chen, *Senior Member, IEEE,* Ning Ge, *Member, IEEE,* Shi Jin, *Fellow, IEEE,* and Hongbo Zhu

Abstract—The sixth generation (6G) network is envisioned to cover remote areas, with the help of satellites and unmanned aerial vehicles (UAVs). Considering the vastness of remote areas and the sparsity of users therein, we investigate a cognitive satellite-UAV network, where satellites and UAVs coordinately share spectrum to provide low-rate and high-rate services in a complementary manner. Multiple UAVs form a virtual antenna array to serve unevenly distributed users via multiple-input-multiple-output (MIMO) non-orthogonal multiple access (NOMA). An on-demand coverage framework is proposed so as to dynamically focus the communication resources on target users. In the framework, a radio map recording the slowly-varying large-scale channel state information (CSI) is utilized. Different from traditional pilot-based approaches, the large-scale CSI is obtained by a lookup in the radio map per the position information of users and UAVs, during the online optimization of the network. In this way, the system overhead could be largely reduced. To explore the potential gain of such a framework, we formulate a joint power allocation problem to maximize the minimum user rate, which is not only non-convex but also with implicit expressions. We recast the problem after uncovering its mathematical characteristics, and derive its locally-optimal solution in an iterative manner. Simulation results corroborate that the proposed framework can significantly improve the coverage performance at a low cost.

Index Terms—Cognitive satellite-UAV network, large-scale channel state information (CSI), non-orthogonal multiple access (NOMA), on-demand coverage, unmanned aerial vehicle (UAV).

Wei Feng, Yueshan Lin, and Ning Ge are with the Department of Electronic Engineering, Beijing National Research Center for Information Science and Technology, Tsinghua University, Beijing 100084, China (email: fengwei@tsinghua.edu.cn, lin-ys17@mails.tsinghua.edu.cn, gening@tsinghua.edu.cn).

Yanmin Wang is with the School of Information Engineering, Minzu University of China, Beijing 100041, China (email: wangyanmin@muc.edu.cn).

Jue Wang is with the School of Information Science and Technology, Nantong University, Nantong 226019, China (email: wangjue@ntu.edu.cn).

Yunfei Chen is with the Department of Engineering, University of Durham, Durham DH1 3LE, U.K. (email: yunfei.chen@durham.ac.uk).

Shi Jin is with the National Mobile Communications Research Laboratory, Southeast University, Nanjing 210096, China (email: jinshi@seu.edu.cn).

Hongbo Zhu is with the Coordination Innovative Center of IoT Technology and Application (Jiangsu), Nanjing University of Posts and Telecommunications, Nanjing 210003, China (email: zhuhb@njupt.edu.cn).

I. INTRODUCTION

Although the deployment of current fifth generation (5G) networks is globally well underway, the remote areas are still largely unconnected [1], [2]. This leads to the increasingly crucial *digital divide* problem [3]. In remote areas, we can hardly establish terrestrial communication infrastructures, due to harsh geographical environments and insufficient power supply. Even if we could, a high cost is often incurred. Non-terrestrial communication infrastructures, e.g., satellites [4], [5] and unmanned aerial vehicles (UAVs) [6], thereby become indispensable to tackle this problem. Due to the vastness of remote areas and the typical sparsity of users therein, one may utilize satellites and UAVs in a cognitive and synergistic manner, and design on-demand coverage strategies to focus communication resources on target users. This leads to a cognitive satellite-UAV network (CSUN) with 'oasis'-oriented coverage, which would be more agile and more efficient than conventional 'blanket'-coverage-oriented approaches.

Key practical concerns for designing such a CSUN lie in the following aspects. Firstly, spectrum sharing between satellites and UAVs is necessary to alleviate the spectrum scarcity problem. However, the footprint of satellite is usually large, and the UAV is sometimes dynamically moving. This leads to more dynamic and more complex co-channel interference than conventional cognitive radio within terrestrial communication infrastructures. Secondly, a UAV swarm is often required, as a single UAV is insufficient for covering vast areas sometimes, due to its limited payload. However, more UAVs generally lead to more complexity. Thirdly, the access distance of different remote-area users varies a lot, which requires agile multiple access technologies. This further complicates the on-demand coverage design.

The aforementioned concerns motivate a CSUN consisting of satellites and multiple UAVs, working in a shared spectrum. The UAVs coordinately form a virtual antenna array to serve unevenly distributed users via multiple-input-multiple-output (MIMO) non-orthogonal multiple access (NOMA). In this particular CSUN, channel state information (CSI) is crucial for satellite-UAV interference mitigation, multi-UAV coordinated transmission, and NOMA design, all of which are vital to achieve on-demand coverage. However, instantaneous CSI acquisition in such CSUNs will render a large amount of system overhead, and is therefore challenging in practice, especially when the channel varies quickly. To tackle this problem, a pre-established radio map recording the large-scale CSI from historical and/or specially measured channel data can

be used. During the online optimization of the network, one may obtain large-scale CSI via simply looking up the radio map, according to the position information of target users and UAVs. In this vision, we need a new optimization framework to exploit the large-scale CSI, paving the way for utilizing radio maps for on-demand coverage.

A. Related Works

1) Satellite-UAV Integration: Using current technologies, neither satellites nor UAVs are capable of providing on-demand coverage in remote areas on their own. As shown in [2], satellites are good at wide-area coverage, but their communication rate is relatively low. UAVs may provide high-rate transmissions if they fly to users as closely as required, but the size of the coverage area is usually limited. Some researchers have thus focused on satellite-UAV coordination [7], while skillfully exploiting the unique features of dedicated Internet-of-Things applications [8]. For instance, Zhang *et al.* [9] considered a hybrid satellite-UAV network where UAVs receive signals from the satellite and relay them to ground users based on the decode-and-forward protocol. Kong *et al.* [10] further adopted a selective decode-and-forward protocol in a downlink UAV relay system, where the satellite signals with low signal-to-noise ratio are removed at the UAV. Yao *et al.* [11] used the UAV to relay delay-sensitive data, e.g., the disaster warning information, to the satellite for realtime applications. In similar scenarios, Lee *et al.* [12] leveraged the multi-agent Reinforcement Learning approach to reduce energy consumption. Li *et al.* [13] optimized the trajectory and power allocation of UAV to enable secure communications between the satellite and ground users in the presence of eavesdroppers. UAV selection was considered for better relaying in the multi-UAV case [14].

In addition to the aforementioned works where UAVs are used as relays, some recent research efforts have been devoted to satellite-UAV spectrum sharing [15]. Li *et al.* [16] improved the coverage performance of a CSUN under the constraint of average interference temperature for spectrum sharing. Luo *et al.* [17] investigated opportunistic spectrum access for UAVs, which share spectrum with both satellites and terrestrial cellular networks. Hua *et al.* [18] optimized the satellite-UAV network with spectrum sharing by cognitive radio techniques. These studies imply that satellite-UAV integration is important, and spectrum sharing between satellites and UAVs is promising to solve the spectrum scarcity problem. In all these works, CSI is indispensable to mitigate the co-channel interference due to spectrum sharing. However, most existing studies have assumed full instantaneous CSI [17], [18], which usually lead to an overwhelming system cost in practice.

2) Multi-UAV Coordination: While most earlier studies have focused on the use of a single UAV [19]–[21], recent research attention has turned to multi-UAV coordination. Wu *et al.* [22] pointed out that the coverage of a single UAV would be limited by its practical payload, size, and power constraints. This problem would become more severe in remote areas, where UAVs may play a critical role in coverage enhancement. For the multi-UAV case, UAVs can work independently to serve different users. For example, Bejaoui *et al.* [23] considered a UAV-user pairing scheme, where in each time slot one UAV pairs with a single user for transmission. Furthermore, Valiulahi *et al.* [24] and Li *et al.* [25] proposed enhanced user association schemes, where each UAV was assigned to cover a group of neighboring users. To avoid inter-UAV interference, Chen *et al.* [26] allocated orthogonal radio resources to UAVs with overlapped coverage.

In addition to user association, multiple UAVs can also coordinately perform signal transmissions. Liu *et al.* [27] presented a coordinated transmission architecture, where multiple UAVs form a virtual antenna array to leverage MIMO technologies for coverage enhancement [28]. Nevertheless, MIMO transmission designs need CSI and most existing studies have assumed full CSI, which may lead to an overwhelming system cost for channel estimation and CSI feedback. Moreover, in remote areas, the CSI exchange among different communication infrastructures become more challenging, due to large-span network topology and spatiotemporal system dynamics. How to perform efficient multi-UAV coordination for CSUNs with limited CSI, is still an open problem.

3) NOMA-Based UAV Communications: In remote areas, users are usually sparsely and unevenly distributed, so that their channel conditions are usually largely different. For such scenarios, traditional orthogonal multiple access (OMA) schemes would inevitably result in a performance loss [29], and NOMA-based communications become promising. For the single-UAV NOMA case, Nasir *et al.* [30] jointly optimized the UAV altitude, the transmit beam-width and radio resource allocation to improve user fairness. Also for better user fairness, Cui *et al.* [31] jointly optimized the UAV trajectory and power allocation. Liu *et al.* [32] maximized the sum rate by jointly optimizing the placement and power allocation of the UAV. Considering the Quality-of-Service (QoS) requirement, Tang *et al.* [33] maximized the number of users with satisfied QoS for NOMA-based UAV communications. Hu *et al.* [34] minimized the total transmit power of a NOMA-based UAV communication system.

In the more practical multi-UAV case, very few works have considered the utilization of NOMA in CSUNs. By assuming that each user is served by at most one UAV, the authors of [35] have investigated the corresponding user-association strategies. Besides, most existing studies [30]–[34] have adopted the free space path loss as the simplified channel model, which cannot precisely characterize the usually-harsh propagation conditions in remote areas.

4) Radio Map: In traditional cognitive radio networks, the radio map was designed for agile spectrum access [36]. It typically stored multi-domain information abstracted from geolocation database, spectrum occupation, propagation environment, and so on. Another typical application of the radio map is fingerprint-based localization [37]. For this purpose, both crowdsourced received signal strength (RSS) measurements and sophisticated updating schemes would be crucial to tackle the environmental dynamics. To reduce the cost for establishing a radio map, some researchers have devoted to radio map interpolation by using, e.g., tailored ray-tracing acceleration [38]. These studies have corroborated the

promising benefits of using radio map in indoor [39] and urban environments [40]. They also shed lights on the utilization of radio maps in remote areas. However, in remote areas, maintaining an update-to-date fine-grained radio map would become more challenging, due to the much larger spatial-temporal dynamics [41]. For example, the building map can be used to improve the construction accuracy of radio map for urban environments [42]. Contrarily, the accurate geographic information for an open and vast remote area is usually hard to acquire.

In light of the aforementioned studies and the unique characteristics of remote areas, we use a coarse-grained radio map in this work, which records the large-scale CSI only, rather than the RSS data [36], [37], [39], [40]. The large-scale CSI varies slowly and usually is easy to obtain in practice. Inevitably, without the small-scale CSI, there would be a performance loss. The goal of this paper is to explore the potential gain by using the large-scale CSI only, and show the pathway of obtaining this gain. Note that, how to construct an accurate radio map for the considered scenario still remains open and is out of the scope of this paper. Both geographic information and machine learning methods could be utilized towards this end in the future work. Since the remote area is usually vast, radio map interpolation should also be considered so as to maintain the updating under the dynamic movement of both satellites and UAVs.

B. Main Contributions

This work investigates a more general CSUN towards on-demand coverage. Unlike [17], [18], [27] that relied on full CSI, we only assume the availability of large-scale CSI at the transmitters. Also, unlike [30]–[34] that focused on a single UAV, the utilization of NOMA is considered in the more powerful multi-UAV case. Besides, a composite channel model consisting of both large-scale and small-scale channel fading is adopted, which is more practical than the free space path loss model [30]–[34]. The main contributions of this paper are summarized as follows.

1) A practical and general model for CSUNs is proposed, where satellites and UAVs coordinately share spectrum to cover low-rate and high-rate users, respectively. Multiple UAVs form a virtual antenna array to serve unevenly distributed users via MIMO-NOMA. Motivated by practical applications, a composite channel model consisting of both large-scale and small-scale channel fading is considered. We use a pre-established radio map, which records the large-scale CSI from historical and/or specially measured channel data. Only the large-scale CSI, obtained via looking up the radio map, is used for on-demand coverage optimization.

2) A joint power allocation problem is formulated to maximize the minimum user rate for on-demand coverage optimization. The problem is proved to be non-convex with intractable implicit expressions. By leveraging the random matrix theory and the successive convex optimization tools, we propose an iterative algorithm to solve the problem. Further, the convergence of the algorithm is proved.

3) Based on the solution to the optimization problem, a power allocation scheme is derived, which can focus communication energy on target users at a largely-reduced system cost. It is observed that although the radio map established based on large-scale CSI only fails to characterize some detailed channel dynamics, it could still be used to achieve a significant improvement in the on-demand coverage framework.

The rest of this paper is organized as follows. We introduce the system model and problem formulation in Section II. In Section III, we solve the problem in an iterative way and accordingly derive a power allocation scheme for radio-map-based on-demand coverage optimization. Then, in Section IV, We provide simulation results and discussions. Conclusions will finally be given in Section V.

II. SYSTEM MODEL AND PROBLEM FORMULATION

As shown in Fig. 1, we consider a practical and general CSUN, where a satellite and N UAVs coordinately share spectrum to cover low-rate and high-rate users, respectively. All UAVs form a virtual antenna array to serve unevenly distributed users via MIMO-NOMA. The high-rate users are grouped into pairs of two users for NOMA transmission. Different pairs are served by orthogonal resource blocks.

Without loss of generality, we focus on an arbitrary pair of users, namely $U^{(1)}$ and $U^{(2)}$. We assume that $U^{(1)}$ directly decodes its own message, while $U^{(2)}$ performs successive interference cancellation (SIC) before decoding its message. The number of antennas equipped at each high-rate user is assumed as N, which is the same as the number of UAVs. Due to spectrum sharing, signals from the UAV swarm will possibly interfere satellite users, i.e., the low-rate users, which are denoted as $U_S^{(j)}, j = 1, ..., J$. Note that the interference from satellite to high-rate users also exist, which however is relatively weak and can be ignored. A radio map is established in advance, we obtain the large-scale CSI by looking up the radio map according to the position of target users, i.e., $U^{(1)}$, $U^{(2)}$, and $U_S^{(j)}, j = 1, ..., J$.

The received signal at $U^{(k)}, k = 1, 2$, can be expressed as

$$\mathbf{y}^{(k)} = \mathbf{H}^{(k)} \sum_{m=1}^{2} \mathbf{x}^{(m)} + \mathbf{n}^{(k)}, \tag{1}$$

where $\mathbf{H}^{(k)} \in \mathbb{C}^{N \times N}$ represents the channel matrix between the UAV swarm and user $U^{(k)}$, and $\mathbf{x}^{(m)} \in \mathbb{C}^{N \times 1}$ denotes the transmitted signal of user $U^{(m)}$, and $\mathbf{n}^{(k)} \in \mathbb{C}^{N \times 1}$ is the additive white Gaussian noise with independently and identically distributed (i.i.d.) entries according to $\mathcal{CN}(0, \sigma^2)$. We define

$$\mathbf{P}^{(k)} = \mathbf{E}\left[\mathbf{x}^{(k)}\mathbf{x}^{(k)H}\right] = \text{diag}\left\{P_1^{(k)}, ..., P_N^{(k)}\right\}, \tag{2}$$

where $P_n^{(k)}$ represents the transmit power of the n-th UAV to $U^{(k)}$. We have

$$P_n^{(k)} \geq 0, \ k = 1, 2, \ n = 1, ..., N, \tag{3}$$

$$P_n^{(1)} + P_n^{(2)} \leq P_{max}, \ n = 1, ..., N, \tag{4}$$

where P_{max} is the maximum transmit power of each UAV.

This article has been accepted for publication in IEEE Transactions on Cognitive Communications and Networking. This is the author's version which has not been fully edited and content may change prior to final publication. Citation information: DOI 10.1109/TCCN.2023.3345857
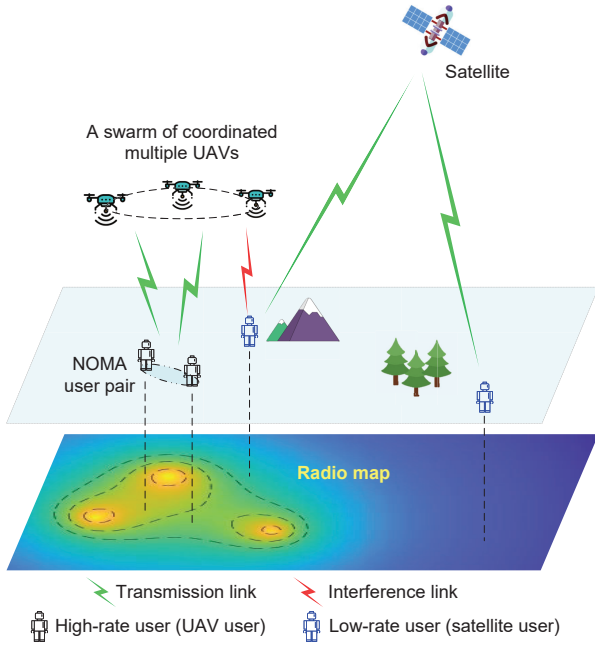
4

Fig. 1. Illustration of a general CSUN, where satellites and UAVs coordinately share spectrum to cover low-rate and high-rate users, respectively. Multiple UAVs form a virtual antenna array and serve unevenly distributed users via MIMO-NOMA. A radio map is established in advance, which records the per-position large-scale CSI for on-demand coverage optimization.

The channel from the UAV swarm to $U^{(k)}$ is modeled as

$$\mathbf{H}^{(k)} = \mathbf{S}^{(k)}\mathbf{L}^{(k)}, \tag{5}$$

where $\mathbf{S}^{(k)} \in \mathbb{C}^{N \times N}$ denotes the Rayleigh small-scale fading with i.i.d. entries according to $\mathcal{CN}(0,1)$, and $\mathbf{L}^{(k)} = \text{diag}\{l_1^{(k)}, ..., l_N^{(k)}\}$ denotes the slowly-varying large-scale channel fading. $l_n^{(k)}$ can be modeled as [43]

$$l_n^{(k)} = 10^{-\frac{1}{20}\left(\frac{A}{1+a\cdot e^{-b(\theta_n^{(k)}-a)}}+B_n^{(k)}\right)}, \tag{6}$$

where

$$A = \eta_{LoS} - \eta_{NLoS}, \tag{7}$$

$$B_n^{(k)} = \eta_{NLoS} + 20\log_{10}\left(\frac{4\pi f d_n^{(k)}}{c}\right). \tag{8}$$

$\eta_{LoS}, \eta_{NLoS}, a$ and b are constant parameters per propagation environments. $d_n^{(k)}$ and $\theta_n^{(k)}$ denote the distance and elevation angle between the n-th UAV and $U^{(k)}$, respectively. f denotes the carrier frequency and c is the speed of light.

Likewise, we express the channel from the UAV swarm to $U_S^{(j)}, j = 1, ..., J$, as

$$\mathbf{H}_S^{(j)} = \mathbf{s}_S^{(j)}\mathbf{L}_S^{(j)}, \tag{9}$$

$$\mathbf{L}_S^{(j)} = \text{diag}\{l_{S,1}^{(j)}, ..., l_{S,N}^{(j)}\}. \tag{10}$$

Since we can only obtain the large-scale CSI from the radio map, we have to carefully handle the unknown small-scale fading. In practice, the leakage interference from UAV swarm to satellite users would act as extra 'background noise'. To

derive the total 'noise' power, we can calculate the average power of interference by taking the expectation operation over the unknown small-scale fading as

$$I_S^{(j)} = \mathbf{E}_{\mathbf{s}_S^{(j)}}\left[\mathbf{H}_S^{(j)}\left(\mathbf{P}^{(1)} + \mathbf{P}^{(2)}\right)\left(\mathbf{H}_S^{(j)}\right)^H\right]$$
$$= \sum_{n=1}^{N}\left(P_n^{(1)} + P_n^{(2)}\right)\left(l_{S,n}^{(j)}\right)^2. \tag{11}$$

Under the spectrum-sharing regime, the satellite users have a maximum tolerable average power of leakage interference, which is determined by their capability of fighting noise, and is called interference temperature in this work. We denote it as I_0. Then, we have

$$I_S^{(j)} = \sum_{n=1}^{N}\left(P_n^{(1)} + P_n^{(2)}\right)\left(l_{S,n}^{(j)}\right)^2 \le I_0, \ j = 1, ...J. \tag{12}$$

According to the principle of MIMO-NOMA, the achievable ergodic rate of $U^{(1)}$ should be

$$R^{(1)} = \min\left(R^{(1\to 1)}, R^{(2\to 1)}\right), \tag{13}$$

where $R^{(1\to 1)}(\mathbf{P}^{(1)}, \mathbf{P}^{(2)})$ and $R^{(2\to 1)}(\mathbf{P}^{(1)}, \mathbf{P}^{(2)})$ are shown in (14) and (15), respectively (on the top of the next page). With perfect SIC, the achievable ergodic rate of $U^{(2)}$ should be

$$R^{(2)} = R^{(2\to 2)}(\mathbf{P}^{(2)})$$
$$= \mathbf{E}_{\mathbf{H}^{(2)}}\left[\log_2\det\left(\mathbf{I}_N + \frac{1}{\sigma^2}\mathbf{H}^{(2)}\mathbf{P}^{(2)}\mathbf{H}^{(2)H}\right)\right]. \tag{16}$$

We compare on-demand coverage with conventional blanket coverage in Fig. 2. For on-demand coverage, the focus of coverage dynamically changes with the position of target users. This is quite different from conventional blanket coverage, by which the network statically covers all areas, regardless of the user's positions. Due to the vastness of remote areas, one has to focus limited communication resources, e.g., transmit power, on target users, so as to achieve desirable high-rate services. This relies on the on-demand coverage strategy, under which the covered area is just like the oasis of desert. Thus, we call also on-demand coverage as oasis-oriented coverage. Toward realizing this vision, to focus communication energy on target users, we maximize the minimum achievable ergodic rate of high-rate users, under transmit power constraints and leakage interference constraints, as

$$\max_{\mathbf{P}^{(1)}, \mathbf{P}^{(2)}} \ \min\left(R^{(1)}, R^{(2)}\right) \tag{17a}$$

$$s.t. \ P_n^{(k)} \ge 0, \ k = 1, 2, \ n = 1, ..., N, \tag{17b}$$

$$P_n^{(1)} + P_n^{(2)} \le P_{max}, \ n = 1, ..., N, \tag{17c}$$

$$\sum_{n=1}^{N}\left(P_n^{(1)} + P_n^{(2)}\right)\left(l_{S,n}^{(j)}\right)^2 \le I_0, \ j = 1 \sim J, \tag{17d}$$

which is challenging due to its non-convexity and the implicit expressions of $R^{(1\to 1)}(\mathbf{P}^{(1)}, \mathbf{P}^{(2)})$, $R^{(2\to 1)}(\mathbf{P}^{(1)}, \mathbf{P}^{(2)})$ and $R^{(2\to 2)}(\mathbf{P}^{(2)})$. In the following, we will tackle these difficulties in a divide-and-conquer manner.
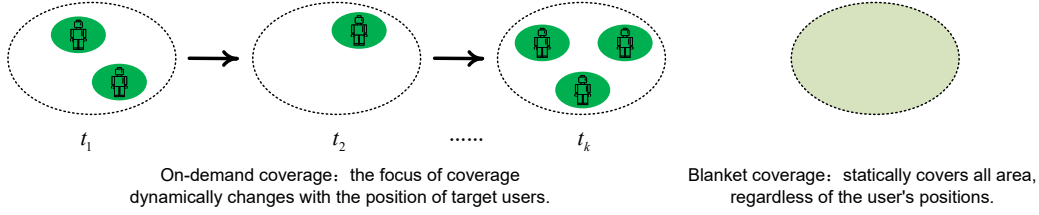
Fig. 2. On-demand coverage versus conventional blanket coverage.

$$R^{(1\to1)}(\mathbf{P}^{(1)}, \mathbf{P}^{(2)}) = \mathbf{E}_{\mathbf{H}^{(1)}}\left[\log_2 \det\left(\mathbf{I}_N + \left(\sigma^2\mathbf{I}_N + \mathbf{H}^{(1)}\mathbf{P}^{(2)}\mathbf{H}^{(1)^H}\right)^{-1}\mathbf{H}^{(1)}\mathbf{P}^{(1)}\mathbf{H}^{(1)^H}\right)\right]. \tag{14}$$

$$R^{(2\to1)}(\mathbf{P}^{(1)}, \mathbf{P}^{(2)}) = \mathbf{E}_{\mathbf{H}^{(2)}}\left[\log_2 \det\left(\mathbf{I}_N + \left(\sigma^2\mathbf{I}_N + \mathbf{H}^{(2)}\mathbf{P}^{(2)}\mathbf{H}^{(2)^H}\right)^{-1}\mathbf{H}^{(2)}\mathbf{P}^{(1)}\mathbf{H}^{(2)^H}\right)\right]. \tag{15}$$

III. POWER ALLOCATION FOR ON-DEMAND COVERAGE

We introduce a slack variable r and recast the problem as

$$\max_{r,\mathbf{P}^{(1)},\mathbf{P}^{(2)}} r \tag{18a}$$

$$s.t. \quad r \le R^{(1\to1)}(\mathbf{P}^{(1)}, \mathbf{P}^{(2)}), \tag{18b}$$

$$r \le R^{(2\to1)}(\mathbf{P}^{(1)}, \mathbf{P}^{(2)}), \tag{18c}$$

$$r \le R^{(2\to2)}(\mathbf{P}^{(2)}), \tag{18d}$$

$$(17b), (17c), (17d),$$

which turns to be more tractable, as the remaining difficulties all lie in the right-side of (18b)-(18d), i.e., $R^{(1\to1)}(\mathbf{P}^{(1)}, \mathbf{P}^{(2)})$, $R^{(2\to1)}(\mathbf{P}^{(1)}, \mathbf{P}^{(2)})$ and $R^{(2\to2)}(\mathbf{P}^{(2)})$. We observe that $R^{(1\to1)}(\mathbf{P}^{(1)}, \mathbf{P}^{(2)})$, $R^{(2\to1)}(\mathbf{P}^{(1)}, \mathbf{P}^{(2)})$ and $R^{(2\to2)}(\mathbf{P}^{(2)})$ have similar substructures, on which we can further regularize the optimization problem. Thus, in the following, we will first unify the forms of $R^{(1\to1)}(\mathbf{P}^{(1)}, \mathbf{P}^{(2)})$, $R^{(2\to1)}(\mathbf{P}^{(1)}, \mathbf{P}^{(2)})$ and $R^{(2\to2)}(\mathbf{P}^{(2)})$ as simple combinations of a general function $R(\mathbf{P}, \mathbf{L})$. Then, in Subsection A, we will introduce an accurate approximation of $R(\mathbf{P}, \mathbf{L})$ to simplify its expression. A new function transformation will be proposed in Subsection B, which brings about desirable monotonic functions that can help to handle the non-convexity of (18b)-(18d). Meanwhile, we also introduce a slack variable $\mathbf{t}$, which although increases the dimension of optimization variables, but successfully makes the problem easy to optimize. Accordingly, in Subsection C, we resort to the first-order Taylor expansion to solve the problem in an iterative way.

Define

$$R_1^{(1\to1)}(\mathbf{P}^{(1)}, \mathbf{P}^{(2)})$$
$$= \mathbf{E}\left[\log_2 \det\left(\mathbf{I}_N + \frac{1}{\sigma^2}\mathbf{H}^{(1)}\left(\mathbf{P}^{(1)} + \mathbf{P}^{(2)}\right)\mathbf{H}^{(1)^H}\right)\right], \tag{19}$$

$$R_2^{(1\to1)}(\mathbf{P}^{(2)})$$
$$= \mathbf{E}\left[\log_2 \det\left(\mathbf{I}_N + \frac{1}{\sigma^2}\mathbf{H}^{(1)}\mathbf{P}^{(2)}\mathbf{H}^{(1)^H}\right)\right]. \tag{20}$$

Then, from (14), we have

$$R^{(1\to1)}(\mathbf{P}^{(1)}, \mathbf{P}^{(2)})$$
$$= R_1^{(1\to1)}(\mathbf{P}^{(1)}, \mathbf{P}^{(2)}) - R_2^{(1\to1)}(\mathbf{P}^{(2)}). \tag{21}$$

Likewise, we rewrite $R^{(2\to1)}$ as

$$R^{(2\to1)}(\mathbf{P}^{(1)}, \mathbf{P}^{(2)})$$
$$= R_1^{(2\to1)}(\mathbf{P}^{(1)}, \mathbf{P}^{(2)}) - R_2^{(2\to1)}(\mathbf{P}^{(2)}), \tag{22}$$

where

$$R_1^{(2\to1)}(\mathbf{P}^{(1)}, \mathbf{P}^{(2)})$$
$$= \mathbf{E}\left[\log_2 \det\left(\mathbf{I}_N + \frac{1}{\sigma^2}\mathbf{H}^{(2)}\left(\mathbf{P}^{(1)} + \mathbf{P}^{(2)}\right)\mathbf{H}^{(2)^H}\right)\right], \tag{23}$$

$$R_2^{(2\to1)}(\mathbf{P}^{(2)})$$
$$= \mathbf{E}\left[\log_2 \det\left(\mathbf{I}_N + \frac{1}{\sigma^2}\mathbf{H}^{(2)}\mathbf{P}^{(2)}\mathbf{H}^{(2)^H}\right)\right]. \tag{24}$$

We unify the forms of (16), (19), (20), (23), and (24) as

$$R(\mathbf{P}, \mathbf{L}) = \mathbf{E}_{\mathbf{H}}\left[\log_2 \det\left(\mathbf{I}_N + \frac{1}{\sigma^2}\mathbf{H}\mathbf{P}\mathbf{H}^H\right)\right]$$
$$= \mathbf{E}_{\mathbf{S}}\left[\log_2 \det\left(\mathbf{I}_N + \frac{1}{\sigma^2}\mathbf{S}\mathbf{L}\mathbf{P}\mathbf{L}\mathbf{S}^H\right)\right], \tag{25}$$

where $\mathbf{P} = \text{diag}\{P_1, ..., P_N\}$, $\mathbf{L} = \text{diag}\{l_1, ..., l_N\}$, and $\mathbf{S} \in \mathbb{C}^{N\times N}$ is with i.i.d. entries according to $\mathcal{CN}(0, 1)$. It is obvious that

$$R^{(1\to1)} = R(\mathbf{P}^{(1)} + \mathbf{P}^{(2)}, \mathbf{L}^{(1)}) - R(\mathbf{P}^{(2)}, \mathbf{L}^{(1)}), \tag{26}$$

$$R^{(2\to1)} = R(\mathbf{P}^{(1)} + \mathbf{P}^{(2)}, \mathbf{L}^{(2)}) - R(\mathbf{P}^{(2)}, \mathbf{L}^{(2)}), \tag{27}$$

$$R^{(2\to2)} = R(\mathbf{P}^{(2)}, \mathbf{L}^{(2)}). \tag{28}$$

We consequently recast (18) as

$$\max_{r,\mathbf{P}^{(1)},\mathbf{P}^{(2)}} r \tag{29a}$$

$$s.t. \quad r \le R(\mathbf{P}^{(1)} + \mathbf{P}^{(2)}, \mathbf{L}^{(1)}) - R(\mathbf{P}^{(2)}, \mathbf{L}^{(1)}), \tag{29b}$$

$$r \le R(\mathbf{P}^{(1)} + \mathbf{P}^{(2)}, \mathbf{L}^{(2)}) - R(\mathbf{P}^{(2)}, \mathbf{L}^{(2)}), \tag{29c}$$

$$r \le R(\mathbf{P}^{(2)}, \mathbf{L}^{(2)}), \tag{29d}$$

$(17b), (17c), (17d).$

A. Approximation of $R(\mathbf{P}, \mathbf{L})$

To remove the expectation operator in $R(\mathbf{P}, \mathbf{L})$, we approximate it by using the random matrix theory as [44]

$$R(\mathbf{P}, \mathbf{L}) \approx \widetilde{R}(\mathbf{P}, u, \mathbf{L}) = \sum_{n=1}^{N} \log_2 \left(1 + \frac{NP_n l_n^2}{u\sigma^2} \right)$$
$$+ N \left[\log_2 u - \log_2 e \left(1 - \frac{1}{u} \right) \right], \quad (30)$$

where u satisfies

$$u \geq 1, \quad (31)$$

$$1 - \frac{1}{u} = \sum_{n=1}^{N} \frac{P_n l_n^2}{\sigma^2 u + NP_n l_n^2}. \quad (32)$$

(30)-(32) can be derived directly according to the *Theorem 1* in [45].

We define $g(\mathbf{P}, u, \mathbf{L})$ as

$$g(\mathbf{P}, u, \mathbf{L}) = 1 - \frac{1}{u} - \sum_{n=1}^{N} \frac{P_n l_n^2}{\sigma^2 u + NP_n l_n^2}, \quad (33)$$

and one has

$$g(\mathbf{P}, u, \mathbf{L}) = 0, \quad (34)$$

which is equivalent to (32). Because this approximation is quite accurate (as shown in Appendix A), we substitute $\widetilde{R}(\mathbf{P}, u, \mathbf{L})$ for $R(\mathbf{P}, \mathbf{L})$, and accordingly recast (29) as

$$\max_{r, \mathbf{P}^{(1)}, \mathbf{P}^{(2)}, \mathbf{u}} r \quad (35a)$$
$$s.t. \quad r \leq \widetilde{R}(\mathbf{P}^{(1)} + \mathbf{P}^{(2)}, u_1^{(1 \to 1)}, \mathbf{L}^{(1)})$$
$$- \widetilde{R}(\mathbf{P}^{(2)}, u_2^{(1 \to 1)}, \mathbf{L}^{(1)}), \quad (35b)$$
$$r \leq \widetilde{R}(\mathbf{P}^{(1)} + \mathbf{P}^{(2)}, u_1^{(2 \to 1)}, \mathbf{L}^{(2)})$$
$$- \widetilde{R}(\mathbf{P}^{(2)}, u_2^{(2 \to 1)}, \mathbf{L}^{(2)}), \quad (35c)$$
$$r \leq \widetilde{R}(\mathbf{P}^{(2)}, u^{(2 \to 2)}, \mathbf{L}^{(2)}), \quad (35d)$$
$$g(\mathbf{P}^{(1)} + \mathbf{P}^{(2)}, u_1^{(1 \to 1)}, \mathbf{L}^{(1)}) = 0, \quad (35e)$$
$$g(\mathbf{P}^{(2)}, u_2^{(1 \to 1)}, \mathbf{L}^{(1)}) = 0, \quad (35f)$$
$$g(\mathbf{P}^{(1)} + \mathbf{P}^{(2)}, u_1^{(2 \to 1)}, \mathbf{L}^{(2)}) = 0, \quad (35g)$$
$$g(\mathbf{P}^{(2)}, u_2^{(2 \to 1)}, \mathbf{L}^{(2)}) = 0, \quad (35h)$$
$$g(\mathbf{P}^{(2)}, u^{(2 \to 2)}, \mathbf{L}^{(2)}) = 0, \quad (35i)$$
$$\mathbf{u} \geq \mathbf{1}, \quad (35j)$$
$$(17b), (17c), (17d),$$

where $\mathbf{u} = [u_1^{(1 \to 1)}, u_2^{(1 \to 1)}, u_1^{(2 \to 1)}, u_2^{(2 \to 1)}, u^{(2 \to 2)}]^T$ is an introduced slack vector. Because we have replaced five terms in (29), i.e., $R(\mathbf{P}^{(1)} + \mathbf{P}^{(2)}, \mathbf{L}^{(1)})$, $R(\mathbf{P}^{(2)}, \mathbf{L}^{(1)})$, $R(\mathbf{P}^{(1)} + \mathbf{P}^{(2)}, \mathbf{L}^{(2)})$, $R(\mathbf{P}^{(2)}, \mathbf{L}^{(2)})$ in the right side of (29c), and $R(\mathbf{P}^{(2)}, \mathbf{L}^{(2)})$ in the right side of (29d), $\mathbf{u}$ has five entries. (35e)-(35i) are accordingly derived from (34), while (35j) is obtained from (31). Note that in the following subsection, we will further slack (35e)-(35i) by using the monotonicity of $g(\mathbf{P}, u, \mathbf{L})$. The $R(\mathbf{P}^{(2)}, \mathbf{L}^{(2)})$ in the right side of (29c) and

(29d) will be slacked differently due to the minus operator before the $R(\mathbf{P}^{(2)}, \mathbf{L}^{(2)})$ in the right side of (29c). Consequently, we use different approximations to substituting them in (35). Till now, the expectation operators have been eliminated. However, the problem in (35) remains challenging, due to the non-convexity of $\widetilde{R}(\mathbf{P}, u, \mathbf{L})$, and the implicit constraints related to $\mathbf{u}$.

B. Problem Transformation

We define

$$f(\mathbf{P}, u, \mathbf{L}) = \log_2 e \cdot \sum_{n=1}^{N} \left[\log \left(1 + \frac{NP_n l_n^2}{\sigma^2 u} \right) \right.$$
$$\left. - \frac{NP_n l_n^2}{\sigma^2 u + NP_n l_n^2} \right] + N \log_2 u. \quad (36)$$

From (30) and (33), we observe that when $g(\mathbf{P}, u, \mathbf{L}) = 0$,

$$f(\mathbf{P}, u, \mathbf{L}) = \widetilde{R}(\mathbf{P}, u, \mathbf{L}). \quad (37)$$

Thus, (35) can be recast as

$$\max_{r, \mathbf{P}^{(1)}, \mathbf{P}^{(2)}, \mathbf{u}} r \quad (38a)$$
$$s.t. \quad r \leq f(\mathbf{P}^{(1)} + \mathbf{P}^{(2)}, u_1^{(1 \to 1)}, \mathbf{L}^{(1)})$$
$$- f(\mathbf{P}^{(2)}, u_2^{(1 \to 1)}, \mathbf{L}^{(1)}), \quad (38b)$$
$$r \leq f(\mathbf{P}^{(1)} + \mathbf{P}^{(2)}, u_1^{(2 \to 1)}, \mathbf{L}^{(2)})$$
$$- f(\mathbf{P}^{(2)}, u_2^{(2 \to 1)}, \mathbf{L}^{(2)}), \quad (38c)$$
$$r \leq f(\mathbf{P}^{(2)}, u^{(2 \to 2)}, \mathbf{L}^{(2)}), \quad (38d)$$
$$(35e) - (35j), (17b), (17c), (17d).$$

We further give the following **Theorem 1**.

Theorem 1: *When $u > 1$, $f(\mathbf{P}, u, \mathbf{L})$ is monotonically increasing with respect to u.*

Proof: See Appendix B. $\square$

From (33), one also observes that $g(\mathbf{P}, u, \mathbf{L})$ is also monotonically increasing with respect to u when $u > 1$. Consequently, we can further transform the problem as

$$\max_{r, \mathbf{P}^{(1)}, \mathbf{P}^{(2)}, \mathbf{u}} r \quad (39a)$$
$$s.t. \quad r \leq f(\mathbf{P}^{(1)} + \mathbf{P}^{(2)}, u_1^{(1 \to 1)}, \mathbf{L}^{(1)})$$
$$- f(\mathbf{P}^{(2)}, u_2^{(1 \to 1)}, \mathbf{L}^{(1)}), \quad (39b)$$
$$r \leq f(\mathbf{P}^{(1)} + \mathbf{P}^{(2)}, u_1^{(2 \to 1)}, \mathbf{L}^{(2)})$$
$$- f(\mathbf{P}^{(2)}, u_2^{(2 \to 1)}, \mathbf{L}^{(2)}), \quad (39c)$$
$$r \leq f(\mathbf{P}^{(2)}, u^{(2 \to 2)}, \mathbf{L}^{(2)}), \quad (39d)$$
$$g(\mathbf{P}^{(1)} + \mathbf{P}^{(2)}, u_1^{(1 \to 1)}, \mathbf{L}^{(1)}) \leq 0, \quad (39e)$$
$$g(\mathbf{P}^{(2)}, u_2^{(1 \to 1)}, \mathbf{L}^{(1)}) \geq 0, \quad (39f)$$
$$g(\mathbf{P}^{(1)} + \mathbf{P}^{(2)}, u_1^{(2 \to 1)}, \mathbf{L}^{(2)}) \leq 0, \quad (39g)$$
$$g(\mathbf{P}^{(2)}, u_2^{(2 \to 1)}, \mathbf{L}^{(2)}) \geq 0, \quad (39h)$$
$$g(\mathbf{P}^{(2)}, u^{(2 \to 2)}, \mathbf{L}^{(2)}) \leq 0, \quad (39i)$$
$$(35j), (17b), (17c), (17d).$$

This article has been accepted for publication in IEEE Transactions on Cognitive Communications and Networking. This is the author's version which has not been fully edited and content may change prior to final publication. Citation information: DOI 10.1109/TCCN.2023.3345857

7

Equivalence between the problem in (39) and that in (38) is shown in the following **Proposition 1**.

Proposition 1: *The problem in (38) and that in (39) are equivalent.*

Proof: The difference between (38) and (39) lies in constraints (39e)-(39i). If equality holds in (39e)-(39i) when (39) is optimized, then the two problems are equivalent. In following, we use the method of proof by contradiction to verify this assumption.

We assume that (39) is optimized at $\mathbf{x}^A = [r^A, \mathbf{P}^{(1),A}, \mathbf{P}^{(2),A}, u_1^{(1\to1),A}, u_2^{(1\to1),A}, u_1^{(2\to1),A}, u_2^{(2\to1),A}, u^{(2\to2),A}]$. If the equality does not hold in (39e), i.e.,

$$g(\mathbf{P}^{(1),A} + \mathbf{P}^{(2),A}, u_1^{(1\to1),A}, \mathbf{L}^{(1)}) < 0, \quad (40)$$

then, there must exist a $u_1^{(1\to1),B} > u_1^{(1\to1),A}$ which satisfies

$$g(\mathbf{P}^{(1),A} + \mathbf{P}^{(2),A}, u_1^{(1\to1),A}, \mathbf{L}^{(1)})$$
$$< g(\mathbf{P}^{(1),A} + \mathbf{P}^{(2),A}, u_1^{(1\to1),B}, \mathbf{L}^{(1)}) = 0. \quad (41)$$

This is because of two facts. One is that g is continuous, and is monotonically increasing with respect to $u_1^{(1\to1)}$. The other is that $g \to 1$ when $u_1^{(1\to1)} \to \infty$.

Further from **Theorem 1**, we know that f is monotonically increasing with $u_1^{(1\to1)}$, which derives

$$f(\mathbf{P}^{(1),A} + \mathbf{P}^{(2),A}, u_1^{(1\to1),A}, \mathbf{L}^{(1)})$$
$$< f(\mathbf{P}^{(1),A} + \mathbf{P}^{(2),A}, u_1^{(1\to1),B}, \mathbf{L}^{(1)}). \quad (42)$$

Thus, there must exist a $r^B \geq r^A$ that satisfies (39c)-(39d), and

$$r^B \leq f(\mathbf{P}^{(1),A} + \mathbf{P}^{(2),A}, u_1^{(1\to1),B}, \mathbf{L}^{(1)})$$
$$- f(\mathbf{P}^{(2),A}, u_2^{(1\to1),A}, \mathbf{L}^{(1)}). \quad (43)$$

$r^B > r^A$ holds if equality does not hold in (39c)-(39d).

From the above analysis, we find that $\mathbf{x}^B = [r^B, \mathbf{P}^{(1),A}, \mathbf{P}^{(2),A}, u_1^{(1\to1),B}, u_2^{(1\to1),A}, u_1^{(2\to1),A}, u_2^{(2\to1),A}, u^{(2\to2),A}]$ also lies in the feasible region of (39), and follows a larger r. This contradicts the hypothesis that $\mathbf{x}^A$ is optimal. Accordingly, we conclude the all equality should hold in (39e)-(39i) when (39) is optimized, and the proposition is therefore proved. $\square$

The problem in (39) is still non-convex. From (36), we obtain

$$f(\mathbf{P}, u, \mathbf{L}) = \log_2 e \cdot \sum_{n=1}^{N} \left[-\log\left(1 - \frac{NP_n l_n^2}{\sigma^2 u + NP_n l_n^2}\right) - \frac{NP_n l_n^2}{\sigma^2 u + NP_n l_n^2} \right] + N\log_2 u. \quad (44)$$

Let

$$F(\mathbf{t}, u) = \log_2 e \cdot \sum_{n=1}^{N} \left[-\log(1 - t_n) - t_n \right] + N\log_2 u. \quad (45)$$

Obviously, when $t_n = \frac{NP_n l_n^2}{\sigma^2 u + NP_n l_n^2}, n = 1, ..., N$, $F(\mathbf{t}, u) = f(\mathbf{P}, u)$. The monotonic property of F with respect to $\mathbf{t}$ is shown in the following **Theorem 2**.

Theorem 2: *when $0 < t_n < 1$, $F(\mathbf{t}, u)$ is monotonically increasing with respect to $t_n, n = 1, ..., N$.*

Proof: See Appendix C. $\square$

Let $\mathbf{t} = [\mathbf{t}_1^{(1\to1)}, \mathbf{t}_2^{(1\to1)}, \mathbf{t}_1^{(2\to1)}, \mathbf{t}_2^{(2\to1)}, \mathbf{t}^{(2\to2)}]$. We transform the problem as

$$\max_{r, \mathbf{P}^{(1)}, \mathbf{P}^{(2)}, \mathbf{u}, \mathbf{t}} r \quad (46a)$$

$$s.t. \quad r \leq F(\mathbf{t}_1^{(1\to1)}, u_1^{(1\to1)}) - F(\mathbf{t}_2^{(1\to1)}, u_2^{(1\to1)}), \quad (46b)$$

$$r \leq F(\mathbf{t}_1^{(2\to1)}, u_1^{(2\to1)}) - F(\mathbf{t}_2^{(2\to1)}, u_2^{(2\to1)}), \quad (46c)$$

$$r \leq F(\mathbf{t}^{(2\to2)}, u^{(2\to2)}), \quad (46d)$$

$$1 - \frac{1}{u_1^{(1\to1)}} \leq \frac{1}{N}\sum_{n=1}^{N} t_{1,n}^{(1\to1)}, \quad (46e)$$

$$1 - \frac{1}{u_2^{(1\to1)}} \geq \frac{1}{N}\sum_{n=1}^{N} t_{2,n}^{(1\to1)}, \quad (46f)$$

$$1 - \frac{1}{u_1^{(2\to1)}} \leq \frac{1}{N}\sum_{n=1}^{N} t_{1,n}^{(2\to1)}, \quad (46g)$$

$$1 - \frac{1}{u_2^{(2\to1)}} \geq \frac{1}{N}\sum_{n=1}^{N} t_{2,n}^{(2\to1)}, \quad (46h)$$

$$1 - \frac{1}{u^{(2\to2)}} \leq \frac{1}{N}\sum_{n=1}^{N} t_n^{(2\to2)}, \quad (46i)$$

$$t_{1,n}^{(1\to1)} \leq \frac{N(P_n^{(1)} + P_n^{(2)})(l_n^{(1)})^2}{\sigma^2 u_1^{(1\to1)} + N(P_n^{(1)} + P_n^{(2)})(l_n^{(1)})^2}, \quad (46j)$$

$$t_{2,n}^{(1\to1)} \geq \frac{NP_n^{(2)}(l_n^{(1)})^2}{\sigma^2 u_2^{(1\to1)} + NP_n^{(2)}(l_n^{(1)})^2}, \quad (46k)$$

$$t_{1,n}^{(2\to1)} \leq \frac{N(P_n^{(1)} + P_n^{(2)})(l_n^{(2)})^2}{\sigma^2 u_1^{(2\to1)} + N(P_n^{(1)} + P_n^{(2)})(l_n^{(2)})^2}, \quad (46l)$$

$$t_{2,n}^{(2\to1)} \geq \frac{NP_n^{(2)}(l_n^{(2)})^2}{\sigma^2 u_2^{(2\to1)} + NP_n^{(2)}(l_n^{(2)})^2}, \quad (46m)$$

$$t_n^{(2\to2)} \leq \frac{NP_n^{(2)}(l_n^{(2)})^2}{\sigma^2 u^{(2\to2)} + NP_n^{(2)}(l_n^{(2)})^2}, \quad (46n)$$

$$\mathbf{0} < \mathbf{t} < \mathbf{1}, \quad (46o)$$

$$(35j), (17b), (17c), (17d), \quad (46p)$$

where $\mathbf{t}_1^{(1\to1)}, \mathbf{t}_2^{(1\to1)}, \mathbf{t}_1^{(2\to1)}, \mathbf{t}_2^{(2\to1)}, \mathbf{t}^{(2\to2)}$ are all $N \times N$ vectors, and (46o) assures that the condition of **Theorem 2** holds.

The equivalence between (39) and (46) can be proved using the same method for **Proposition 1**. In short, since F is monotonically increasing with respect to t_n, (46) will maximize $t_{1,n}^{(1\to1)}, t_{1,n}^{(2\to1)}, t_n^{(2\to2)}$ while minimize $t_{2,n}^{(1\to1)}, t_{2,n}^{(2\to1)}$. Therefore, the equality in all constraints (46j)-(46n) will hold, and the problem is equivalent to that in (39).

C. Iterative Solution

We solve (46) in an iterative manner via resorting to the successive convex optimization approach. All non-convex terms in each constraint are substituted with their first-order Taylor expansions.

From (45), we observe that function F is concave with respect to u, and is convex to $t_n, n = 1, ..., N$. Thus, constraints (46b)-(46d) are non-convex. The first-order Taylor expansion of F at a certain $\tilde{u}$ can be derived as

$$F_u(\mathbf{t}, u|\tilde{u}) = \log_2 \mathrm{e} \cdot \sum_{n=1}^{N} [-\log(1 - t_n) - t_n]$$
$$+ N \log_2 \mathrm{e} \cdot \left[\log(\tilde{u}) + \frac{(u - \tilde{u})}{\tilde{u}} \right]. \quad (47)$$

The first-order Taylor expansion of F at a certain $\tilde{\mathbf{t}}$ can be derived as

$$F_t(\mathbf{t}, u|\tilde{\mathbf{t}}) = \log_2 \mathrm{e} \cdot \sum_{n=1}^{N} \left[-\log\left(1 - \tilde{t}_n\right) \right.$$
$$\left. + \frac{\tilde{t}_n}{1 - \tilde{t}_n}(t_n - 1) \right] + N \log_2 u. \quad (48)$$

Consequently, the constraints (46b)-(46d) can be replaced by

$$r \le F_t(\mathbf{t}_1^{(1\to1)}, u_1^{(1\to1)}|\tilde{\mathbf{t}}_1^{(1\to1)})$$
$$- F_u(\mathbf{t}_2^{(1\to1)}, u_2^{(1\to1)}|\tilde{u}_2^{(1\to1)}), \quad (49)$$

$$r \le F_t(\mathbf{t}_1^{(2\to1)}, u_1^{(2\to1)}|\tilde{\mathbf{t}}_1^{(2\to1)})$$
$$- F_u(\mathbf{t}_2^{(2\to1)}, u_2^{(2\to1)}|\tilde{u}_2^{(2\to1)}), \quad (50)$$

$$r \le F_t(\mathbf{t}^{(2\to2)}, u^{(2\to2)}|\tilde{\mathbf{t}}^{(2\to2)}). \quad (51)$$

The constraints (46e), (46g), and (46i) can be replaced by

$$1 - \left(\frac{1}{\tilde{u}_1^{(1\to1)}} - \frac{u_1^{(1\to1)} - \tilde{u}_1^{(1\to1)}}{\left(\tilde{u}_1^{(1\to1)}\right)^2} \right) \le \frac{1}{N} \sum_{n=1}^{N} t_{1,n}^{(1\to1)}, \quad (52)$$

$$1 - \left(\frac{1}{\tilde{u}_1^{(2\to1)}} - \frac{u_1^{(2\to1)} - \tilde{u}_1^{(2\to1)}}{\left(\tilde{u}_1^{(2\to1)}\right)^2} \right) \le \frac{1}{N} \sum_{n=1}^{N} t_{1,n}^{(2\to1)}, \quad (53)$$

$$1 - \left(\frac{1}{\tilde{u}^{(2\to2)}} - \frac{u^{(2\to2)} - \tilde{u}^{(2\to2)}}{\left(\tilde{u}^{(2\to2)}\right)^2} \right) \le \frac{1}{N} \sum_{n=1}^{N} t_n^{(2\to2)}. \quad (54)$$

The constraints (46j)-(46n) are non-convex. Take (46j) and (46k) as examples. (46j) can be equivalently transformed as

$$\log(N(l_n^{(1)})^2) + \log(P_n^{(1)} + P_n^{(2)}) + \log(1 - t_{1,n}^{(1\to1)})$$
$$\ge \log(u_1^{(1\to1)}) + \log(t_{1,n}^{(1\to1)}) + \log(\sigma^2), \quad (55)$$

where $\log(u_1^{(1\to1)})$ and $\log(t_{1,n}^{(1\to1)})$ are non-convex terms. Similarly, (46k) becomes

$$\log(N(l_n^{(1)})^2) + \log(P_n^{(2)}) + \log(1 - t_{2,n}^{(1\to1)})$$
$$\le \log(u_2^{(1\to1)}) + \log(t_{2,n}^{(1\to1)}) + \log(\sigma^2), \quad (56)$$

where $\log(P_n^{(2)})$ and $\log(1 - t_{2,n}^{(1\to1)})$ are non-convex terms.

After performing Taylor expansion, (55)-(56) can be replaced by (57)-(58) (shown on the top of the next page).

Likewise, we derive the convex approximations for constraints (46l)-(46n), by replacing all non-convex terms with their Taylor expansions, as shown in (59)-(61) (on the top of the next page).

Algorithm 1 Iterative power allocation algorithm for on-demand coverage.

Input: N, $\mathbf{L}^{(1)}$, $\mathbf{L}^{(2)}$, P_{max}, σ^2, ϵ
1: *Initialization*: $P_n^{(1),0} = \frac{1}{2}P_{max}$, $P_n^{(2),0} = \frac{1}{2}P_{max}$, $n = 1, ..., N$, $u_1^{(1\to1),0} = 1$, $u_1^{(2\to1),0} = 1$, $u^{(2\to2),0} = 1$,
$u_2^{(1\to1),0} = \frac{1}{2} + \frac{1}{2}\sqrt{1 + \frac{2NP_{max}}{\sigma^2} \cdot \max_{1 \le n \le N}\left(l_n^{(1)}\right)^2}$,
$u_2^{(2\to1),0} = \frac{1}{2} + \frac{1}{2}\sqrt{1 + \frac{2NP_{max}}{\sigma^2} \cdot \max_{1 \le n \le N}\left(l_n^{(2)}\right)^2}$,
$t_{1,n}^{(1\to1),0} = \frac{NP_{max}\left(l_n^{(1)}\right)^2}{\sigma^2 u_1^{(1\to1),0} + NP_{max}\left(l_n^{(1)}\right)^2}$, $n = 1, ..., N$
$t_{2,n}^{(1\to1),0} = \frac{NP_{max}\left(l_n^{(1)}\right)^2}{2\sigma^2 u_2^{(1\to1),0} + NP_{max}\left(l_n^{(1)}\right)^2}$, $n = 1, ..., N$
$t_{1,n}^{(2\to1),0} = \frac{NP_{max}\left(l_n^{(2)}\right)^2}{\sigma^2 u_1^{(2\to1),0} + NP_{max}\left(l_n^{(2)}\right)^2}$, $n = 1, ..., N$
$t_{2,n}^{(2\to1),0} = \frac{NP_{max}\left(l_n^{(2)}\right)^2}{2\sigma^2 u_2^{(2\to1),0} + NP_{max}\left(l_n^{(2)}\right)^2}$, $n = 1, ..., N$
$t_n^{(2\to2),0} = \frac{NP_{max}\left(l_n^{(2)}\right)^2}{\sigma^2 u^{(2\to2),0} + NP_{max}\left(l_n^{(2)}\right)^2}$, $n = 1, ..., N$.
2: *Iterations*: $s = 1, 2, ...,$
3: **repeat**
4:     Calculate r^s, $\mathbf{P}^{(1),s}$, $\mathbf{P}^{(2),s}$ via solving problem (62),
5: **until** $\frac{|r^s - r^{s-1}|}{r^{s-1}} < \epsilon$.
Output: $\mathbf{P}^{(1),s}, \mathbf{P}^{(2),s}$

The above Taylor expansion operations lead to an iterative process to solve the problem. If the locally-optimal solution in the $(s - 1)$-th iteration is $[r^{s-1}, \mathbf{P}^{(1),s-1}, \mathbf{P}^{(2),s-1}, \mathbf{u}^{s-1}, \mathbf{t}^{s-1}]$, we then solve the following optimization problem in the s-th iteration

$$\max_{r, \mathbf{P}^{(1)}, \mathbf{P}^{(2)}, \mathbf{u}, \mathbf{t}} r \quad (62a)$$
$$s.t. \quad (35j), (46f), (46h)$$
$$(17b), (17c), (17d), (49) - (54), (57) - (61). \quad (62b)$$

This iterative algorithm is summarized in **Algorithm 1**. Its convergence is shown in the following **Theorem 3**.

Theorem 3: *In Algorithm 1, the optimization objective r is non-decreasing with the iteration, and thus the algorithm is assured to converge.*

Proof: See Appendix D. $\qquad \square$

IV. SIMULATION RESULTS AND DISCUSSION

We consider a CSUN consisting of a satellite and $N = 5$ UAVs. Without loss of generality, we assume that the UAVs are uniformly deployed in a three-dimensional cylindrical area, denoted as C_1 with $\{[x, y, z]^T | \sqrt{x^2 + y^2} \le 4000\ m, 700 \le z \le 1300\ m\}$. $U^{(1)}$ is placed at $\mathbf{c}^{(1)} = [10000, 0, 0]^T m$, and $U^{(2)}$ is placed at $\mathbf{c}^{(2)} = [0, 0, 0]^T m$. A total of $J = 5$ satellite users, which encounter the leakage interference from UAVs, are uniformly dropped in the area $C_S = \{[x, y, 0]^T | \sqrt{x^2 + y^2} \le 20000\ m\}$. The interference temperature limitation is set to be $I_0 = -88$ dBm. Channel parameters $(\eta_{LoS}, \eta_{NLoS}, a, b)$ are set as $(0.1, 21, 4.8860, 0.4290)$ [43]. Simulation results are

$$\log\left(N\left(l_n^{(1)}\right)^2\right) + \log\left(P_n^{(1)} + P_n^{(2)}\right) + \log\left(1 - t_{1,n}^{(1\to1)}\right)$$
$$\geq \left[\log\left(\tilde{u}_1^{(1\to1)}\right) + \frac{u_1^{(1\to1)} - \tilde{u}_1^{(1\to1)}}{\tilde{u}_1^{(1\to1)}}\right] + \left[\log\left(\tilde{t}_{1,n}^{(1\to1)}\right) + \frac{t_{1,n}^{(1\to1)} - \tilde{t}_{1,n}^{(1\to1)}}{\tilde{t}_{1,n}^{(1\to1)}}\right] + \log(\sigma^2). \tag{57}$$

$$\log\left(N\left(l_n^{(1)}\right)^2\right) + \left[\log\left(\tilde{P}_n^{(2)}\right) + \frac{P_n^{(2)} - \tilde{P}_n^{(2)}}{\tilde{P}_n^{(2)}}\right] + \left[\log\left(1 - \tilde{t}_{2,n}^{(1\to1)}\right) - \frac{t_{2,n}^{(1\to1)} - \tilde{t}_{2,n}^{(1\to1)}}{1 - \tilde{t}_{2,n}^{(1\to1)}}\right]$$
$$\leq \log\left(u_2^{(1\to1)}\right) + \log\left(t_{2,n}^{(1\to1)}\right) + \log(\sigma^2). \tag{58}$$

$$\log\left(N\left(l_n^{(2)}\right)^2\right) + \log\left(P_n^{(1)} + P_n^{(2)}\right) + \log\left(1 - t_{1,n}^{(2\to1)}\right)$$
$$\geq \left[\log\left(\tilde{u}_1^{(2\to1)}\right) + \frac{u_1^{(2\to1)} - \tilde{u}_1^{(2\to1)}}{\tilde{u}_1^{(2\to1)}}\right] + \left[\log\left(\tilde{t}_{1,n}^{(2\to1)}\right) + \frac{t_{1,n}^{(2\to1)} - \tilde{t}_{1,n}^{(2\to1)}}{\tilde{t}_{1,n}^{(2\to1)}}\right] + \log(\sigma^2). \tag{59}$$

$$\log\left(N\left(l_n^{(2)}\right)^2\right) + \left[\log\left(\tilde{P}_n^{(2)}\right) + \frac{P_n^{(2)} - \tilde{P}_n^{(2)}}{\tilde{P}_n^{(2)}}\right] + \left[\log\left(1 - \tilde{t}_{2,n}^{(2\to1)}\right) - \frac{t_{2,n}^{(2\to1)} - \tilde{t}_{2,n}^{(2\to1)}}{1 - \tilde{t}_{2,n}^{(2\to1)}}\right]$$
$$\leq \log\left(u_2^{(2\to1)}\right) + \log\left(t_{2,n}^{(2\to1)}\right) + \log(\sigma^2). \tag{60}$$

$$\log\left(N\left(l_n^{(2)}\right)^2\right) + \log\left(P_n^{(2)}\right) + \log\left(1 - t_n^{(2\to2)}\right)$$
$$\geq \left[\log\left(\tilde{u}^{(2\to2)}\right) + \frac{u^{(2\to2)} - \tilde{u}^{(2\to2)}}{\tilde{u}^{(2\to2)}}\right] + \left[\log\left(\tilde{t}_n^{(2\to2)}\right) + \frac{t_n^{(2\to2)} - \tilde{t}_n^{(2\to2)}}{\tilde{t}_n^{(2\to2)}}\right] + \log(\sigma^2). \tag{61}$$

Fig. 3. Convergence performance of the proposed algorithm.

Fig. 4. Minimum ergodic rate of users, changing with the maximum transmit power for each UAV, achieved by different schemes.

averaged over 50 snapshots. In each snapshot, the positions of UAVs and satellite users are independently generated. By such setup, we might average the influence of UAV topology, and show that our method applies to any logical UAV topology.

In Fig. 3, we evaluate the convergence performance of the proposed algorithm. The number of iterations required is shown for the randomly-selected 50 snapshots. For all cases, the proposed algorithm converges within 12 iterations. This verifies **Theorem 3**, and also shows the practical value of the proposed algorithm in resource-limited applications.

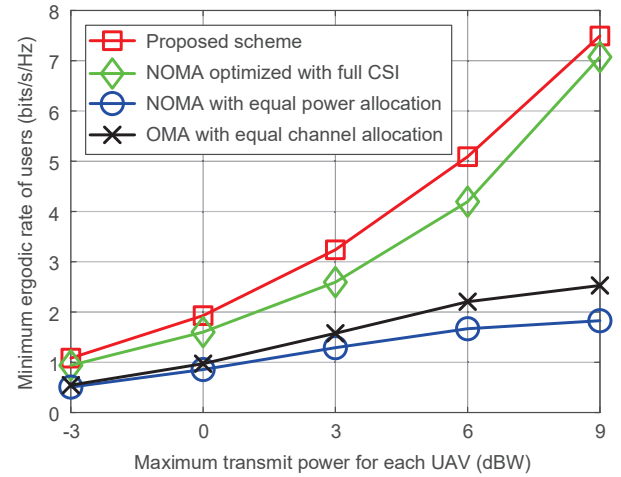In Fig. 4, we depict the minimum ergodic rate achieved by

different algorithms. The compared methods include

- *NOMA optimized with full CSI*: The algorithm proposed in [30], which was designed with full CSI.
- *NOMA with equal power allocation:* NOMA transmission, and equal power allocation between $U^{(1)}$ and $U^{(2)}$.
- *OMA with equal channel allocation:* OMA transmission, and equal channel allocation between $U^{(1)}$ and $U^{(2)}$.

From Fig. 4, one observes that the proposed algorithm and the algorithm proposed in [30] outperform the other two schemes. Intuitively, with equal power/channel allocation, the user with worse channel condition is allocated with inadequate
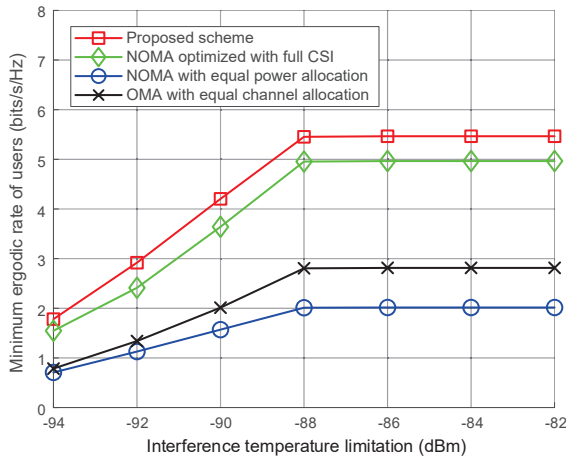
Fig. 5. Minimum ergodic rate of users, changing with the interference temperature limitation, achieved by different schemes.
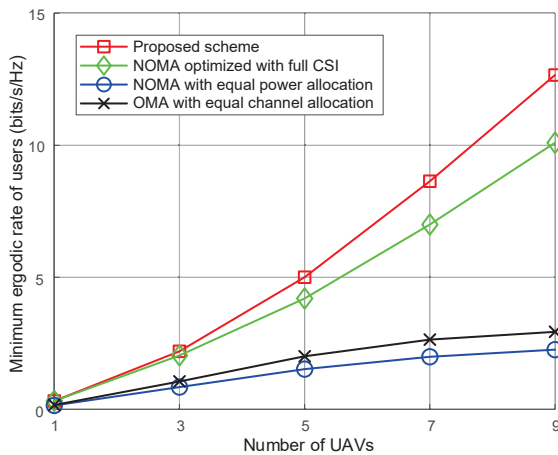

Fig. 6. Minimum ergodic rate of users, changing with the number of UAVs, achieved by different schemes.
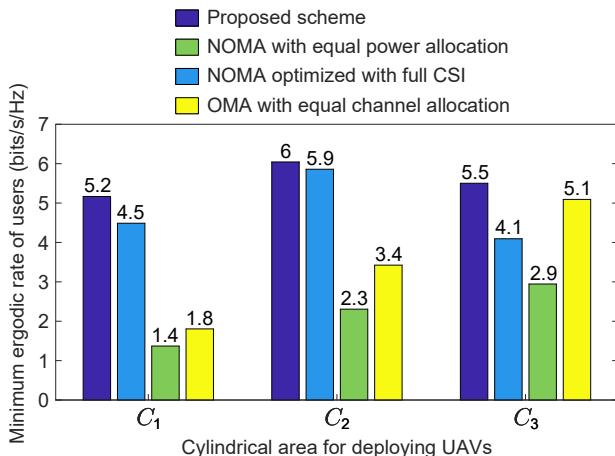

Fig. 7. Minimum ergodic rate of users achieved by different UAV deployment.

resources, which leads to poor user fairness. This runs counter to the goal of on-demand coverage. It can also be observed that the proposed scheme achieves higher minimum ergodic rate than the scheme proposed in [30]. The reason is that the scheme proposed in [30] requires full CSI for optimization, and the CSI imperfectness would bring about performance loss given only the coarse-grained radio map. On the other hand, this corroborates the significance of redesigning power allocation scheme for CSUNs with large-scale CSI only.

We further compare these four schemes in Fig. 5 and Fig. 6. In Fig. 5, we set $P_{max} = 6$ dBW. Similar to Fig. 4, one may observe that the proposed scheme always offers the best performance with different interference temperature limitations. When the limitation goes larger than -88 dBm, the minimum ergodic rate of users would stop growing. Intuitively, for these regions, the maximum transmit power for each UAV becomes the bottleneck factor. In Fig. 6, we also set $P_{max} = 6$ dBW. We can see the superiority of the proposed scheme with different number of UAVs. The always-increasing curves also indicate that more UAVs more performance gains. Besides, the performance gap becomes larger with the increase of UAV number, which confirms that the proposed scheme adapts to large UAV swarms.

We further evaluate the influence of UAV deployment on coverage performance, by comparing three different cylindrical areas, as shown in Table I, in which the UAVs are uniformly distributed. For C_1, the UAVs are close to $U^{(2)}$, which results in distinct channel conditions between $U^{(1)}$ and $U^{(2)}$. For C_3, the access distance from $U^{(1)}$ to UAVs is comparable to that from $U^{(2)}$. C_2 lies in the middle of C_1 and C_3. The minimum ergodic rate are shown in Fig. 7, by setting the maximum transmit power to be 6 dBW. From the figure, we observe that our proposed scheme always achieves the best coverage performance in all of the three cases. This verifies the superiority of our proposed scheme in coverage efficiency. Besides, we observe that the performance gain over the equal power/channel allocation methods for C_1 and C_2 is much more remarkable than that for C_3. This is because when $U^{(1)}$ and $U^{(2)}$ have similar channel conditions, equal channel/power allocation could already achieve a satisfactory coverage performance. Thus, in practice, we should choose appropriate methods according to both system parameters, e.g., network topology, and affordable cost.

In Fig. 8, we evaluate the influence of the number of UAVs on coverage performance. The minimum ergodic rate of users under different number of UAVs is shown in the figure. It is clear that more UAVs yields larger coverage performance gain. This is intuitively reasonable as more UAVs would provide more multiplexing and diversity gain for MIMO-NOMA transmissions. More importantly, this corroborates the promising benefit of leveraging multi-UAV coordination.

We finally show the relationship between the minimum ergodic rate and the interference temperature limitation in Fig. 9. It can be seen that when I_0 is relatively small, different maximum transmit power constraints would lead to similar spectrum sharing performance. In this condition, the leakage interference dominates the co-existence of satellites and UAVs. When the interference temperature limitation becomes large

TABLE I
DIFFERENT CYLINDRICAL AREAS FOR DEPLOYING UAVs.

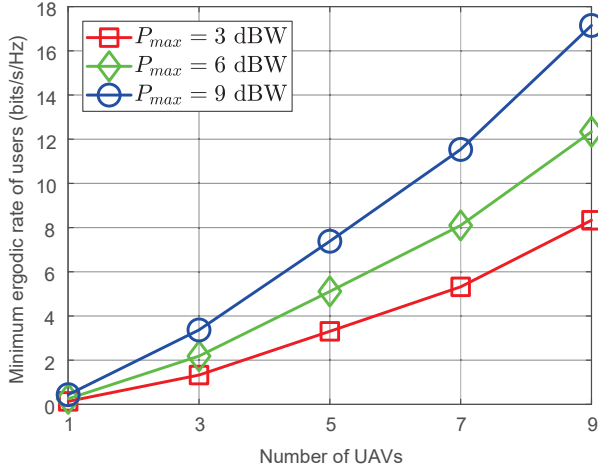| Label	Cylindrical Area
C_1	$\{[x,y,z]^T \mid \sqrt{x^2+y^2} \leq 4000\ m, 700 \leq z \leq 1300\ m\}$
C_2	$\{[x,y,z]^T \mid \sqrt{(x-5000)^2+y^2} \leq 4000\ m, 700 \leq z \leq 1300\ m\}$
C_3	$\{[x,y,z]^T \mid \sqrt{(x-10000)^2+y^2} \leq 4000\ m, 700 \leq z \leq 1300\ m\}$

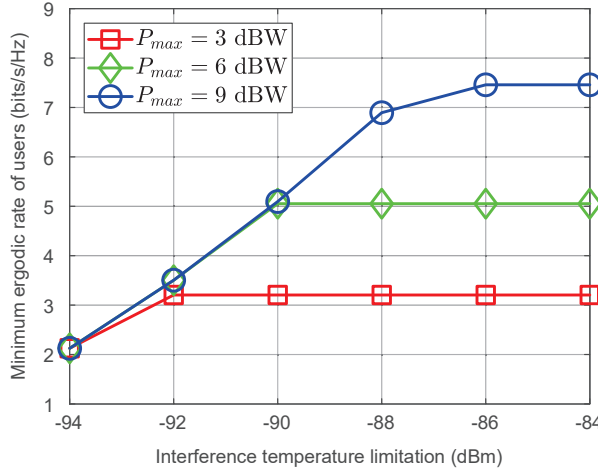Fig. 8. Minimum ergodic rate of users under different number of UAVs, i.e., N.

Fig. 9. Minimum ergodic rate of users under different interference temperature limitation, i.e., I_0.

enough, the transmit power would turn to the main bottleneck, and larger transmit power leads to better coverage performance.

V. CONCLUSIONS

This paper has proposed a practical framework for covering remote areas in an on-demand manner. In this framework, satellites and UAVs coordinately share spectrum to provide low-rate and high-rate services in a complementary manner. Multiple UAVs form a virtual antenna array to serve unevenly distributed users via MIMO-NOMA. To reduce system cost,

we have suggested to look up the large-scale CSI in the pre-established radio map per the position information of users and UAVs, during the online optimization of the network. A joint power allocation scheme has been proposed to maximize the minimum user rate. It used the large-scale CSI only, and was derived with the help of random matrix theory and the successive convex optimization tool. Simulation results have corroborated that the proposed scheme could improve the coverage performance at a low cost. With the proposed framework, a systematic design can be realized to comprehensively consider the UAV deployment, the size of UAV swarm, and the interference temperature limitation in practice.

APPENDIX A
VERIFICATION OF THE ACCURACY OF (30)

Using the approximation of $R(\mathbf{P},\mathbf{L})$ in (30), we can calculate the achievable ergodic rate of $U^{(1)}$ and $U^{(2)}$ according to (13), (26), (27), and (28). We can also adopt Monte Carlo simulations to mimic the expectation operator in the original expression of the achievable ergodic rate according to (14), (15), and (16).

With the same simulation parameters as Section IV, we obtain Fig. 10 and Fig. 11 for comparison. It can be observed that the error of approximation over Monte Carlo simulation results is almost negligible, for all randomly-selected snapshots, for all simulated transmit powers, and for both $U^{(1)}$ and $U^{(2)}$. Thus, the approximation is accurate enough for sequel optimizations.

APPENDIX B
PROOF OF **THEOREM 1**

We take the partial derivative of f with respect to u as

$$
\begin{aligned}
\frac{\partial f(\mathbf{P},u,\mathbf{L})}{\partial u} &= \log_2 e \cdot \sum_{n=1}^{N}\left[\frac{-\frac{NP_n l_n^2}{\sigma^2 u^2}}{1+\frac{NP_n l_n^2}{\sigma^2 u}}\right. \\
&\quad \left.+\frac{NP_n l_n^2 \sigma^2}{(\sigma^2 u+NP_n l_n^2)^2}\right]+N\log_2 e\cdot\frac{1}{u} \\
&= \log_2 e \cdot \sum_{n=1}^{N}\left[\frac{-NP_n l_n^2(\sigma^2 u+NP_n l_n^2)}{u\cdot(\sigma^2 u+NP_n l_n^2)^2}\right. \\
&\quad \left.+\frac{NP_n l_n^2\sigma^2 u}{u\cdot(\sigma^2 u+NP_n l_n^2)^2}+\frac{1}{u}\right] \\
&= \log_2 e \cdot \sum_{n=1}^{N}\frac{\sigma^2\cdot(\sigma^2 u+2NP_n l_n^2)}{(\sigma^2 u+NP_n l_n^2)^2} > 0.
\end{aligned}
$$
(B.1)

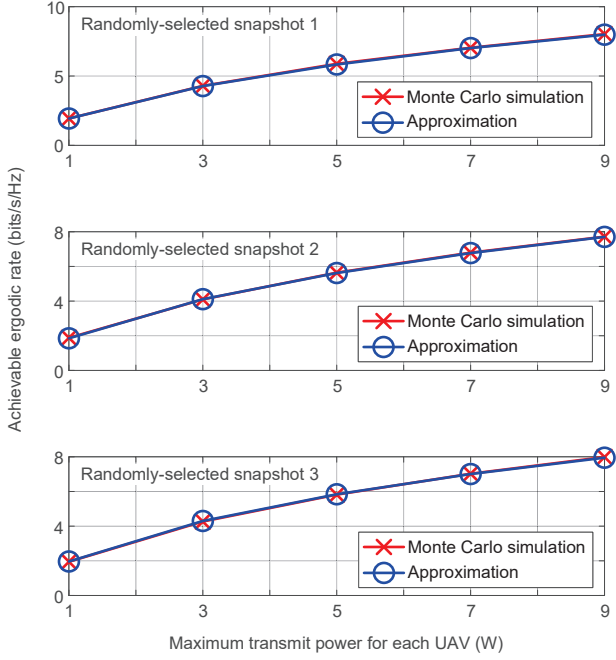Thus, $f(\mathbf{P},u,\mathbf{L})$ is monotonically increasing with u.

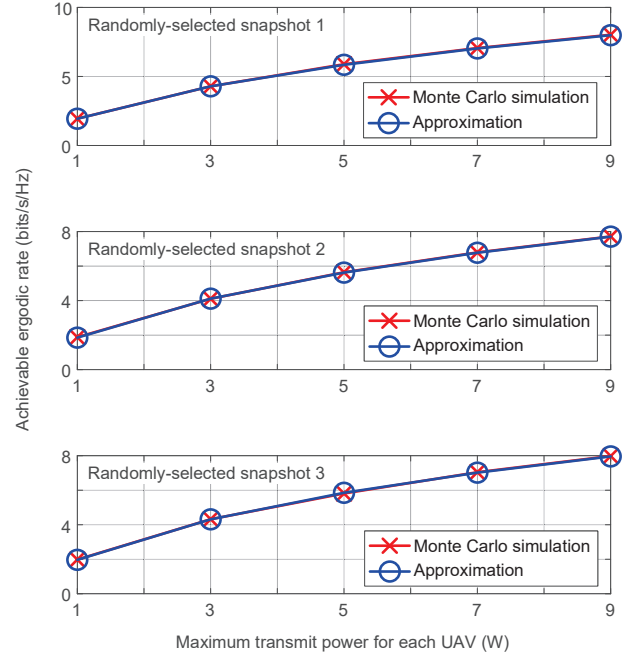Fig. 10. Achievable ergodic rate of $U^{(1)}$ calculated using Monte Carlo simulation and the proposed approximation.

Fig. 11. Achievable ergodic rate of $U^{(2)}$ calculated using Monte Carlo simulation and the proposed approximation.

APPENDIX C
PROOF OF THEOREM 2

We take the partial derivative of F with respect to t_n as

$$\frac{\partial F(\mathbf{t}, u)}{\partial t_n} = \log_2 e \cdot \left(\frac{1}{1 - t_n} - 1 \right)$$
$$= \log_2 e \cdot \frac{t_n}{1 - t_n}. \quad \text{(C.1)}$$

When $0 < t_n < 1$, it is clear that F is monotonically increasing with respect to t_n, $n = 1, ..., N$, which proves the theorem.

APPENDIX D
PROOF OF THEOREM 3

We denote the optimal variables in the $(s-1)$-th and the s-th iterations as $\mathbf{x}^{s-1} = [r^{s-1}, \mathbf{P}^{(1),s-1}, \mathbf{P}^{(2),s-1}, \mathbf{u}^{s-1}, \mathbf{t}^{s-1}]$ and $\mathbf{x}^s = [r^s, \mathbf{P}^{(1),s}, \mathbf{P}^{(2),s}, \mathbf{u}^s, \mathbf{t}^s]$, respectively. $\mathbf{x}^s$ is obtained through solving (62) based on $\mathbf{x}^{s-1}$.

The most convenient method to prove the theorem is through induction. Given that $\mathbf{x}^{s-1}$ is in the feasible region of (46), if we corroborate that $\mathbf{x}^s$ also lies in the feasible region of (46), while $r^s \geq r^{s-1}$ holds, the theorem is then proved.

We first prove that $\mathbf{x}^s$ lies in the feasible region of (46). Since $\mathbf{x}^s$ is obtained via solving (62), it is in the feasible region of (62). From (49), one has

$$r^s \leq F_t(\mathbf{t}_1^{(1 \to 1),s}, u_1^{(1 \to 1),s} \mid \mathbf{t}_1^{(1 \to 1),s-1})$$
$$- F_u(\mathbf{t}_2^{(1 \to 1),s}, u_2^{(1 \to 1),s} \mid u_2^{(1 \to 1),s-1}). \quad \text{(D.1)}$$

Since $\log(u) \leq \log(\tilde{u}) + \frac{u - \tilde{u}}{\tilde{u}}$, $F(\mathbf{t}, u) \leq F_u(\mathbf{t}, u|\tilde{u})$ holds. Since $-\log(1 - t_n)$ is convex, $-\log(1 - t_n) \geq -\log(1 - \tilde{t}_n) +$

$\frac{t_n - \tilde{t}_n}{1 - \tilde{t}_n}$ holds, which further derives that $F(\mathbf{t}, u) \geq F_t(\mathbf{t}, u|\tilde{\mathbf{t}})$. Therefore, from (D.1), one has

$$r^s \leq F(\mathbf{t}_1^{(1 \to 1),s}, u_1^{(1 \to 1),s}) - F(\mathbf{t}_2^{(1 \to 1),s}, u_2^{(1 \to 1),s}), \quad \text{(D.2)}$$

which confirms that $\mathbf{x}^s$ satisfies (46b). Likewise, it can be proved that $\mathbf{x}^s$ also satisfies (46c)-(46d).

From (52), we have

$$1 - \left(\frac{1}{u_1^{(1 \to 1),s-1}} - \frac{u_1^{(1 \to 1),s} - u_1^{(1 \to 1),s-1}}{(u_1^{(1 \to 1),s-1})^2} \right)$$
$$\leq \frac{1}{N} \sum_{n=1}^{N} t_{1,n}^{(1 \to 1),s}. \quad \text{(D.3)}$$

Since $\frac{1}{u}$ is convex, $\frac{1}{u} \geq \left(\frac{1}{\tilde{u}} - \frac{u - \tilde{u}}{(\tilde{u})^2} \right)$ holds, and

$$1 - \frac{1}{u_1^{(1 \to 1),s}} \leq \frac{1}{N} \sum_{n=1}^{N} t_{1,n}^{(1 \to 1),s}, \quad \text{(D.4)}$$

and thus constraint (46e) is satisfied. Likewise, (46g) and (46i) are also satisfied.

From (57), we have (D.5) (shown on the top of the next page), and from (D.5) it can be deduced that (D.6) (shown on the top of the next page) also holds. Therefore, (55) and (46j) are satisfied. Similar process can be carried out to prove that $\mathbf{x}^s$ satisfies (46k)-(46n).

In a nutshell, $\mathbf{x}^s$ lies in the feasible region of (46). Moreover, since the Taylor expansion is conducted at $\mathbf{x}^{s-1}$, which belongs to the feasible region of (62), and $r^s \geq r^{s-1}$ holds. The theorem can be thus proved.

$$\log\left(N\left(l_n^{(1)}\right)^2\right) + \log\left(P_n^{(1),s} + P_n^{(2),s}\right) + \log\left(1 - t_{1,n}^{(1\to 1),s}\right)$$

$$\geq \left[\log\left(u_1^{(1\to 1),s-1}\right) + \frac{u_1^{(1\to 1),s} - u_1^{(1\to 1),s-1}}{u_1^{(1\to 1),s-1}}\right] + \left[\log\left(t_{1,n}^{(1\to 1),s-1}\right) + \frac{t_{1,n}^{(1\to 1),s} - t_{1,n}^{(1\to 1),s-1}}{t_{1,n}^{(1\to 1),s-1}}\right] + \log(\sigma^2). \quad \text{(D.5)}$$

$$\log\left(N\left(l_n^{(1)}\right)^2\right) + \log\left(P_n^{(1),s} + P_n^{(2),s}\right) + \log\left(1 - t_{1,n}^{(1\to 1),s}\right) \geq \log\left(u_1^{(1\to 1),s}\right) + \log\left(t_{1,n}^{(1\to 1),s}\right) + \log(\sigma^2). \quad \text{(D.6)}$$

REFERENCES

[1] O. Onireti, J. Qadir, M. A. Imran, and A. Sathiaseelan, "Will 5G see its blind side? Evolving 5G for universal Internet access," in *Proc. workshop Global Access Internet All*, Aug. 2016, pp. 1–6.

[2] X. Li, W. Feng, J. Wang, Y. Chen, N. Ge, and C.-X. Wang, "Enabling 5G on the ocean: a hybrid satellite-UAV-terrestrial network solution," *IEEE Wireless Commun.*, vol. 27, no. 6, pp. 116–121, Dec. 2020.

[3] H. Saarnisaari, S. Dixit, M.-S. Alouini, et. al., "A 6G white paper on connectivity for remote areas," *6G Flagship White Papers*, arXiv:2004.14699, Apr. 2020.

[4] B. Feng, Y. Huang, A. Tian, H. Wang, H. Zhou, S. Yu, and H. Zhang, "DR-SDSN: an elastic differentiated routing framework for software-defined satellite networks," *IEEE Wireless Commun.*, vol. 29, no. 6, pp. 80–86, Dec. 2022.

[5] X. Fang, W. Feng, T. Wei, Y. Chen, N. Ge, and C.-X. Wang, "5G embraces satellites for 6G ubiquitous IoT: basic models for integrated satellite terrestrial networks," *IEEE Internet Things J.*, vol. 8, no. 18, pp. 14399–14417, Sep. 2021.

[6] Y. Zeng, R. Zhang, and T. J. Lim, "Wireless communications with unmanned aerial vehicles: opportunities and challenges," *IEEE Commun. Mag.*, vol. 54, no. 5, pp. 36–42, May 2016.

[7] Y. Wang, W. Feng, J. Wang, and T. Q. S. Quek, "Hybrid satellite-UAV-terrestrial networks for 6G ubiquitous coverage: a maritime communications perspective," *IEEE J. Sel. Areas Commun.*, vol. 39, no. 11, pp. 3475-3490, Nov. 2021.

[8] B. Feng, A. Tian, S. Yu, J. Li, H. Zhou, and H. Zhang, "Efficient cache consistency management for transient IoT data in content-centric networking," *IEEE Internet Things J.*, vol. 9, no. 15, pp. 12931–12944, Aug. 2022.

[9] S. Zhang and J. Liu, "Analysis and optimization of multiple unmanned aerial vehicle-assisted communications in post-disaster areas," *IEEE Trans. Veh. Tech.*, vol. 67, no. 12, pp. 12049–12060, Dec. 2018.

[10] H. Kong, M. Lin, W. P. Zhu, H. Amindavar, and M. S. Alouini, "Multiuser scheduling for asymmetric FSO/RF links in satellite-UAV-terrestrial networks," *IEEE Wireless Commun. Lett.*, vol. 9, no. 8, pp. 1235-1239, Aug. 2020.

[11] Y. Yao, D. Dong, S. Huang, C. Pan, S. Chen, and X. Li, "Optimization of the Internet of remote things data acquisition based on satellite UAV integrated network," *China Commun.*, vol. 20, no. 7, pp. 15-28, Jul. 2023.

[12] D. Lee, Y. Sun, S. Kim, et al., "Multi-agent reinforcement learning-based resource allocation scheme for UAV-assisted Internet of remote things systems," *IEEE Access*, vol. 11, pp. 53155–53164, 2023.

[13] H. Li, J. Li, M. Liu, and F. Gong, "UAV-assisted secure communication for coordinated satellite-terrestrial networks," *IEEE Commun. Lett.*, vol. 27, no. 7, pp. 1709-1713, Jul. 2023.

[14] P. K. Sharma, D. Deepthi, and D. I. Kim, "Outage probability of 3-D mobile UAV relaying for hybrid satellite-terrestrial networks," *IEEE Commun. Lett.*, vol. 24, no. 2, pp. 418–422, Feb. 2020.

[15] C. Liu, W. Feng, Y. Chen, C.-X. Wang, and N. Ge, "Cell-free satellite-UAV networks for 6G wide-area Internet of Things," *IEEE J. Sel. Areas Commun.*, vol. 39, no. 4, pp. 1116-1131, Apr. 2021.

[16] X. Li, W. Feng, Y. Chen, C. Wang, and N. Ge, "Maritime coverage enhancement using UAVs coordinated with hybrid satellite-terrestrial networks," *IEEE Trans. Commun.*, vol. 68, no. 4, pp. 2355–2369, Apr. 2020.

[17] S. Luo, Y. Xiao, R. Lin, X. Xie, G. Bi, Y. Zhao, and J. Huang, "Opportunistic spectrum access for UAV communications towards ultra dense networks," *IEEE Access*, vol. 7, pp. 175021–175032, 2019.

[18] M. Hua, Y. Wang, M. Lin, C. Li, Y. Huang, and L. Yang, "Joint CoMP transmission for UAV-aided cognitive satellite terrestrial networks," *IEEE Access*, vol. 7, pp. 14959–14968, 2019.

[19] Y. Zeng, R. Zhang, and T. J. Lim, "Throughput maximization for UAV-enabled mobile relaying systems," *IEEE Trans. Commun.*, vol. 64, no. 12, pp. 4983–4996, Dec. 2016.

[20] Q. Wu and R. Zhang, "Common throughput maximization in UAV-enabled OFDMA systems with delay consideration," *IEEE Trans. Commun.*, vol. 66, no. 12, pp. 6614–6627, Dec. 2018.

[21] Y. Chen, W. Feng, and G. Zheng, "Optimum placement of UAV as relays," *IEEE Commun. Lett.*, vol. 22, no. 2, pp. 248-251, Feb. 2018.

[22] Q. Wu, Y. Zeng, and R. Zhang, "Joint trajectory and communication design for multi-UAV enabled wireless networks," *IEEE Trans. Wireless Commun.*, vol. 17, no. 3, pp. 2109–2121, Mar. 2018.

[23] A. Bejaoui, K. Park, and M. Alouini, "A QoS-oriented trajectory optimization in swarming unmanned-aerial-vehicles communications," *IEEE Wireless Commun. Lett.*, vol. 9, no. 6, pp. 791–794, Jun. 2020.

[24] I. Valiulahi and C. Masouros, "Multi-UAV deployment for throughput maximization in the presence of co-channel interference," *IEEE Internet Things J.*, vol. 8, no. 5, pp. 3605–3618, Mar. 2021.

[25] L. Li, X. Wen, Z. Lu, W. Jing, and H. Zhang, "Energy-efficient multi-UAVs deployment and movement for emergency response," *IEEE Commun. Lett.*, vol. 25, no. 5, pp. 1625–1629, May 2021.

[26] R. Chen, X. Li, Y. Sun, S. Li, and Z. Sun, "Multi-UAV coverage scheme for average capacity maximization," *IEEE Commun. Lett.*, vol. 24, no. 3, pp. 653–657, Mar. 2020.

[27] L. Liu, S. Zhang, and R. Zhang, "CoMP in the sky: UAV placement and movement optimization for multi-user communications," *IEEE Trans. Commun.*, vol. 67, no. 8, pp. 5645–5658, Aug. 2019.

[28] W. Feng, Y. Wang, N. Ge, J. Lu, and J. Zhang, "Virtual MIMO in multi-cell distributed antenna systems: coordinated transmissions with large-scale CSIT," *IEEE J. Sel. Areas Commun.*, vol. 31, no. 10, pp. 2067–2081, Oct. 2013.

[29] Y. Liu, Z. Qin, M. Elkashlan, Z. Ding, A. Nallanathan, and L. Hanzo, "Nonorthogonal multiple access for 5G and beyond," *Proc. IEEE*, vol. 105, no. 12, pp. 2347–2381, Dec. 2017.

[30] A. A. Nasir, H. D. Tuan, T. Q. Duong, and H. V. Poor, "UAV-enabled communication using NOMA," *IEEE Trans. Commun.*, vol. 67, no. 7, pp. 5126–5138, Jul. 2019.

[31] F. Cui, Y. Cai, Z. Qin, M. Zhao, and G. Y. Li, "Multiple access for mobile-UAV enabled networks: joint trajectory design and resource allocation," *IEEE Trans. Commun.*, vol. 67, no. 7, pp. 4980-4994, Jul. 2019.

[32] X. Liu, J. Wang, N. Zhao, Y. Chen, S. Zhang, Z. Ding, and F. R. Yu, "Placement and power allocation for NOMA-UAV networks," *IEEE Wireless Commun. Lett.*, vol. 8, no. 3, pp. 965–968, Jun. 2019.

[33] R. Tang, J. Cheng, and Z. Cao, "Joint placement design, admission control, and power allocation for NOMA-based UAV systems," *IEEE Wireless Commun. Lett.*, vol. 9, no. 3, pp. 385–388, Mar. 2020.

[34] D. Hu, Q. Zhang, Q. Li, and J. Qin, "Joint position, decoding order, and power allocation optimization in UAV-based NOMA downlink communications," *IEEE Syst. J.*, vol. 14, no. 2, pp. 2949–2960, Jun. 2020.

[35] T. Hou, Y. Liu, Z. Song, X. Sun, and Y. Chen, "Exploiting NOMA for UAV communications in large-scale cellular networks," *IEEE Trans. Commun.*, vol. 67, no. 10, pp. 6897–6911, Oct. 2019.

[36] H. B. Yilmaz, T. Tugcu, F. Alagöz, and S. Bayhan, "Radio environment map as enabler for practical cognitive radio networks," *IEEE Commun. Mag.*, vol. 51, no. 12, pp. 162–169, Dec. 2013.

[37] B. Huang, Z. Xu, B. Jia, and G. Mao, "An online radio map update scheme for WiFi fingerprint-based localization," *IEEE Internet Things J.*, vol. 6, no. 4, pp. 6909–6918, Aug. 2019.

[38] N. Suga, R. Sasaki, M. Osawa, and T. Furukawa, "Ray tracing acceleration using total variation norm minimization for radio map simulation," *IEEE Wireless Commun. Lett.*, vol. 10, no. 3, pp. 522–526, Mar. 2021.

This article has been accepted for publication in IEEE Transactions on Cognitive Communications and Networking. This is the author's version which has not been fully edited and content may change prior to final publication. Citation information: DOI 10.1109/TCCN.2023.3345857

14

[39] A. M. Rajab and B. Wang, "Automatic radio map database maintenance and updating based on crowdsourced samples for indoor localization," *IEEE Sensors J.*, vol. 22, no. 1, pp. 575–588, Jan. 2022.

[40] Y. Zhang and S. Wang, "K-nearest neighbors gaussian process regression for urban radio map reconstruction," *IEEE Commun. Lett.*, vol. 26, no. 12, pp. 3049–3053, Dec. 2022.

[41] K. Li, C. Li, B. Yu, Z. Shen, Q. Zhang, S. He, and J. Chen, "Model and transfer spatial-temporal knowledge for fine-grained radio map reconstruction," *IEEE Trans. Cogn. Commun. Netw.*, vol. 8, no. 2, pp. 828–841, Jun. 2022.

[42] G. Chen, Y. Liu, T. Zhang, J. Zhang, X. Guo, and J. Yang, "A graph neural network based radio map construction method for urban environment," *IEEE Commun. Lett.*, vol. 27, no. 5, pp. 1327–1331, May 2023.

[43] A. Al-Hourani, S. Kandeepan, and S. Lardner, "Optimal LAP altitude for maximum coverage," *IEEE Wireless Commun. Lett.*, vol. 3, no. 6, pp. 569–572, Dec. 2014.

[44] A. M. Tulino and S. Verdú, "Random matrix theory and wireless communications," *Found. Trends Commun. Inf. Theory*, vol. 1, no. 1, pp. 1–182, 2004.

[45] W. Feng, Y. Li, S. Zhou, J. Wang, and M. Xia, "Downlink capacity of distributed antenna systems in a multi-cell environment," in Proc. *IEEE Wireless Commun. Netw. Conf. (WCNC)*, pp. 1–5, Apr. 2009.

Wei Feng (Senior Member, IEEE) received the B.S. and Ph.D. degrees from the Department of Electronic Engineering, Tsinghua University, Beijing, China, in 2005 and 2010, respectively. He is currently a Professor with the Department of Electronic Engineering, Tsinghua University. His research interests include maritime communication networks, large-scale distributed antenna systems, and coordinated satellite-UAV-terrestrial networks. He serves as the Assistant to the Editor-in-Chief of CHINA COMMUNICATIONS and an Editor of IEEE TRANSACTIONS ON COGNITIVE COMMUNICATIONS AND NETWORKING.

Yueshan Lin received the B.S. degree from the Department of Electronic Engineering, Tsinghua University, Beijing, China, in 2021. He is currently pursuing the Ph.D. degree with the Department of Electronic Engineering, Tsinghua University, Beijing. His research interests include UAV communications, satellite communications and mobile edge computing.

Yanmin Wang received the B.S. degree from Shandong University, China, in 2008, and the Ph.D. degree from the Department of Electronic Engineering, Tsinghua University, Beijing, China, in 2013. She is currently an associate professor at the School of Information Engineering, Minzu University of China. Her research interests include distributed antenna systems, satellite networks, and coordinated satellite-UAV-terrestrial networks.
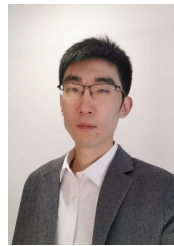
Jue Wang (Member, IEEE) received the B.S. degree in communications engineering from Nanjing University, Nanjing, China, in 2006, the M.S. and Ph. D. degrees from National Communications Research Laboratory, Southeast University, Nanjing, in 2009 and 2014, respectively. From 2014 to 2016, he was with Singapore University of Technology and Design as a Postdoctoral Research Fellow. He is currently with the School of Information Science and Technology, Nantong University, Nantong, China.

Dr. Wang has served as a Technical Program Committee member and a reviewer for a number of IEEE conferences/journals. He was awarded as an Exemplary Reviewer of IEEE TRANSACTIONS ON COMMUNICATIONS in 2014, and Exemplary Reviewer of IEEE WIRELESS COMMUNICATIONS LETTERS in 2021. His research interests include MIMO/Massive MIMO wireless communications, non-terrestrial networks, and machine learning in communication systems.

Yunfei Chen (Senior Member, IEEE) received the B.E. and M.E. degrees in electronics engineering from Shanghai Jiaotong University, Shanghai, China, in 1998 and 2001, respectively, and the Ph.D. degree from the University of Alberta in 2006. He is currently a Professor with the Department of Engineering, University of Durham, U.K. His research interests include wireless communications, cognitive radios, wireless relaying, and energy harvesting.

Ning Ge (Member, IEEE) received the B.S. and Ph.D. degrees from Tsinghua University, China, in 1993 and 1997, respectively. From 1998 to 2000, he was involved in the development of ATM switch fabric ASIC with ADC Telecommunications, Dallas. Since 2000, he has been with the Department of Electronics Engineering, Tsinghua University, where he is currently a FULL PROFESSOR and also serves as the Director of the Communication Institute. His research interests include ASIC design, short range wireless communication, and wireless communications. He is a Senior Member of CIC and CIE.

Shi Jin (Fellow, IEEE) received the B.S. degree in communications engineering from Guilin University of Electronic Technology, Guilin, China, in 1996, the M.S. degree from Nanjing University of Posts and Telecommunications, Nanjing, China, in 2003, and the Ph.D. degree in information and communications engineering from the Southeast University, Nanjing, in 2007. From June 2007 to October 2009, he was a Research Fellow with the Adastral Park Research Campus, University College London, London, U.K. He is currently with the faculty of the National Mobile Communications Research Laboratory, Southeast University. His research interests include wireless communications, random matrix theory, and information theory. He is serving as an Area Editor for the Transactions on Communications and IET Electronics Letters. He was an Associate Editor for the IEEE Transactions on Wireless Communications, and IEEE Communications Letters, and IET Communications. Dr. Jin and his co-authors have been awarded the 2011 IEEE Communications Society Stephen O. Rice Prize Paper Award in the field of communication theory, the IEEE Vehicular Technology Society 2023 Jack Neubauer Memorial Award, the 2022 Best Paper Award and the 2010 Young Author Best Paper Award by the IEEE Signal Processing Society.

Hongbo Zhu received the B.S. degree in communications engineering from the Nanjing University of Posts and Telecommunications, Nanjing, China, in 1982, and the Ph.D. degree in information and communications engineering from the Beijing University of Posts and Telecommunications, Beijing, China, in 1996. He is currently a Professor with the Nanjing University of Posts and Telecommunications. He is also the Head of the Coordination Innovative Center of IoT Technology and Application (Jiangsu), which is the first government authorized Coordination Innovative Center of IoT in China. He also serves as a referee or expert in multiple national organizations and committees. He has authored and co-authored over 200 technical papers published in various journals and conferences. He is currently leading a big group and multiple funds on IoT and wireless communications with current focus on architecture and enabling technologies for Internet of Things. His research interests include mobile communications, wireless communication theory, and electromagnetic compatibility.